Control for Weld Penetration in VPPAW of Aluminum Alloys Using the Front Weld Pool Image Signal

The study shows the feasibility of implementing weld formation control of VPPAW of aluminum in real time

BY B. ZHENG, H. J. WANG, Q. I. WANG AND R. KOVACEVIC

Abstract. This paper presents a technique for real-time, closed-loop feedback control of weld penetration based on the front image signal of the weld pool in variable polarity plasma arc welding (VPPAW) of aluminum alloys. The formation of an image can be acquired when the arc light reflects off the concave, mirror-like surface of the depressed keyhole weld pool and passes through a band-pass filter onto the image sensor. The image of the visual keyhole (nominal keyhole) is a two-dimensional projected picture of the actual keyhole weld pool. The determination of the geometrical size of the nominal keyhole is also described according to the consecutive frames of the image. The variation in size of the nominal keyhole is closely correlated to the bottom diameter of a keyhole. A model of the relationship between the bottom diameter of a keyhole and the geometrical size of the nominal keyhole weld pool in the image is established and examined using the BP artificial neural network theory. A cutting or a keyhole collapse phenomenon is successfully avoided and uniform weld formation is obtained in a welding process using the model to control both the wire feed and the welding current when the thermal conditions of the butt-jointed workpieces are changed. The results achieved show a feasible way to implement the real-time weld formation control into the aluminum VPPAW.

Introduction

Variable polarity plasma arc welding (VPPAW) of aluminum alloys in the keyhole mode has been used successfully in production, such as in fabricating the space shuttle external tanks (Refs. 1–4).

B. ZHENG, H. J. WANG and R. KOVACEVIC are with Southern Methodist University, Dallas, Tex. Q. I. WANG is with Harbin Institute of Technology, Harbin, P. R. China.

Compared with other welding processes, VPPAW can generate high weld quality and high productivity at relatively low cost. These attractive features are attributed mainly to a fully penetrated keyhole-mode weld pool, inside which hydrogen cannot be trapped, and to the removal of tenacious oxide film on the workpiece surface, which guarantees better fluidity of the metal in the weld pool. However, keyhole collapse and melt-through may occur during a welding process if disturbances such as abruptly varying thermal conditions exist, especially when welding plates ranging from 4.0 to 25.4 mm. Thus, selecting process parameters and providing control of the stability of weld formation during welding to produce a satisfactory weld remains a challenge.

One effective approach is to monitor the keyhole weld pool. Recently, it was found the presence or absence of a keyhole could be determined by measuring the ratio of hydrogen to argon in the plasma arc column with an optical spectrometer (Ref. 5). However, the size of the keyhole cannot be determined and the welding process cannot be distinguished from the cutting process according to the signal. At present, two difficult problems are associated with front-face sensing of the keyhole weld pool in plasma arc welding (PAW): inaccessibility of the weld pool because of the limited torch stand-off distance and the interference of the arc radiation. PAW technology in the one-keyhole-per-pulse mode can be fairly well applied to steels, so the arc sound or the arc efflux light from the back side of the workpiece can be used to detect the size of the keyhole. Based on this principle, a full-penetration weld bead has been guaranteed in real-time feedback control (Refs. 6–9). However, this type of technology is not applicable to aluminum alloys. Also, detecting the keyhole from the back side of the workpiece is not feasible in some cases, such as in the welding of pressure vessels. To date, constant parameter open-loop control of weld formation is still being used in PAW of aluminum alloys by the keyhole mode.

Key Words

Aluminum Alloys
VPPAW
Front Image Sensing
Weld Pool
Keyhole Diameter
Neural Networks Model
Penetration Control
Weld Formation

In recent years, welding researchers have focused on using machine vision systems to sense the weld pool for controlling the full penetration state in gas tungsten arc welding (GTAW) and gas metal arc welding (GMAW) (Refs. 10–15). The arc light filtering solution has been investigated through coaxial viewing of the weld pool in GTAW (Ref. 16). These approaches are based on the principle the diffuse reflection of arc light from the mirror-like weld pool surface is weaker than that from the surrounding area. Thus, in the image, the weld pool produces a dark area, while the solid part of the workpiece appears as a bright area. Some researchers used a pulsating laser synchronized with a high-shutter-speed camera to overcome the arc light interference in GTAW of stainless steel (Refs. 17–19). With this approach, a clear image of the weld pool is captured and the weld pool boundary is calculated in real time using a developed image-processing algorithm. The geometrical appearance of the weld pool is characterized by the rear angles and the length

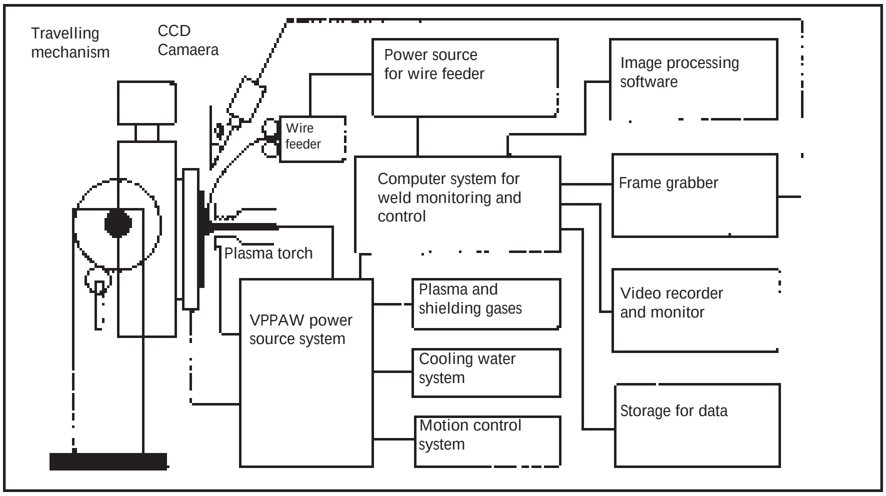

Fig. 1 — Schematic of the monitoring and control system in VPPAW.

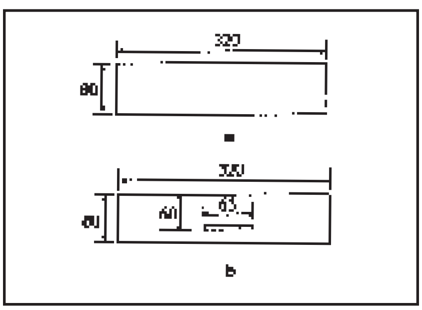

Fig. 2 — Schematic of workpieces. A — Ordinary conditions; B — varied thermal conditions with a slot.

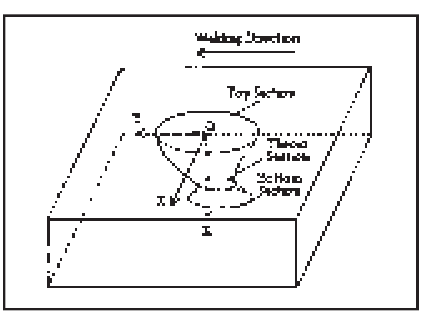

Fig. 3 — Three-dimensional schematic of a keyhole.

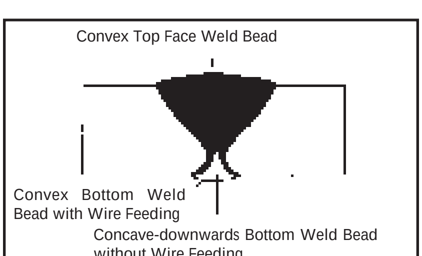

Fig. 4 — Schematic of a weld bead cross section.

of the weld pool. For the full-penetration case, the back weld bead width could be related to the geometrical features of the front side of the weld pool. Infrared thermography has also been extensively investigated (Refs. 20–22). It was found the interference of the bright arc light could be prevented, and the depth of the joint penetration could be determined using the characteristics of the temperature profiles of steel in GTAW. The instantaneous decrease of the welding current has also been used to weaken the intensity of the arc light in order to capture a clear weld pool image during welding (Ref. 23). However, in some cases, this approach may not be acceptable because of the poor weld bead that occurs, such as in PAW of aluminum alloys using the keyhole mode.

Besides the inaccessibility of the weld pool and the arc radiation interference in PAW, a common problem existing in the welding of aluminum alloys is that nearly no color change occurs when the plate is melted. Consequently, the weld pool cannot be easily distinguished from the solid base metal using the visible spectrum range. Thus, processing a weld pool image in the case of aluminum alloys is much more difficult than in the case of steel welding.

Another problem in the welding of aluminum alloys is the tenacious oxide film on aluminum strongly impedes the flow of the weld pool in the welding process so that a very poor weld formation with oxide inclusion is easily generated. A cutting process with an oxidizing surface cut may also occur if the plates are melted through in a plasma arc welding process by the keyhole mode. Actually, the main representation of an unstable weld formation in VPPAW of aluminum alloys is the transition from a keyhole welding process to a cutting process or to a melt-in-mode welding process without a keyhole. Although lots of factors influence the stability of the weld formation, variation in thermal conditions of the workpiece (which is an uncontrollable factor in application) is mainly responsible for the transition if the optimized welding parameters are applied. Therefore, to avoid this transition, the guarantee of the dynamic presence of a keyhole weld pool in a plasma arc welding process with a varied thermal condition is one of the biggest challenges in the control of a quality weld.

Currently, the real-time feedback control of the weld formation using a keyhole signal in PAW of aluminum alloys is still not available, despite its applications to some key products. Therefore, exploration of this research issue is crucial to achieving a quality weld. This paper will focus on front imaging the weld pool to achieve the required signal of a keyhole; establishing the model of the relationship between the bottom diameter of a keyhole and the geometrical size of a weld pool in the image and implementing the real-time feedback control of the weld penetration.

Experimental Procedure

Experimental System

The image sensing system used is shown in Fig. 1. It consists of a commercial CCD camera (15 mm in diameter and 100 mm in length) with a band-pass filter, a monitor, an image processing card, a PC-Pentium computer and a video recorder. The parameters of the filter are the following: center wave length 658 nm, half wave width 10 nm, transmissivity 27% and background depth of field 1/1000. These specific filter parameters are selected because the intensity of the arc light when using argon as the shielding gas is much weaker within the above spectrum. The welding system also shown in Fig. 1 consists of a variable-polarity welding power source, programmable sequence controller, plasma gas controller, CNC positioning system, computer-controlled wire feeder and plasma arc torch. The camera is attached to and positioned in front of the plasma arc torch with its axis at an angle ϕ (43 deg) from the workpiece surface plane.

Experimental Conditions

Variations in the keyhole size can be effected by changing some of the welding conditions such as the welding current, the wire feed speed and the thermal conditions of the plates (the shape of the workpiece, for instance). Since variation in the thermal conditions is crucial to stability of weld formation in the welding of aluminum products, all the experiments were conducted using workpieces with varied thermal conditions, except the experiments done for comparison. Butt-joint welds were made with wire feeding. Two shapes of 5-mm-thick 2024 aluminum plates are shown in Fig. 2. The welding current in the start-up segment reaches 80–90 A within 5 s, which increases up to 90–120 A within 5–10 s from the termination of this segment to the beginning of the main body segment. Other parameters have the following values: a direct current electrode negative (DCEN) to direct current electrode positive (DCEP) time ratio of 22 to 3.0 ms, DCEN current 80–100 A, DCEP current 110–120 A, pilot arc current 15 A, plasma gas flow rate 4.5 L/min, shielding gas flow rate 6 L/min, welding speed 100 mm/min, torch stand-off distance 5 mm, angle of workpiece surface plane to the horizontal plane equal to 85 deg, orifice diameter 3.2 mm, orifice length 3.5 mm and a tungsten electrode setback of 3.2 mm.

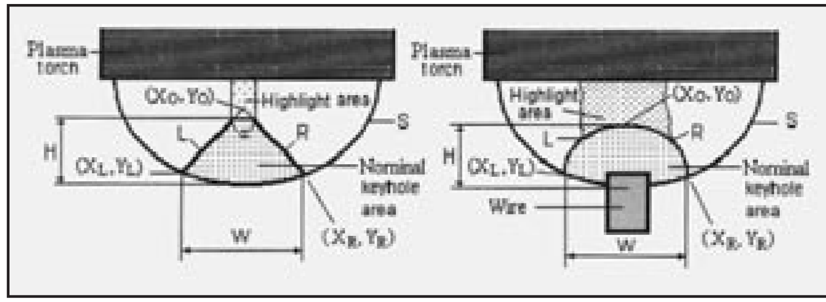

Fig. 5 — Schematic of the normal keyhole weld pool viewed from the top. (S is the front periphery of the keyhole weld pool; R is the right periphery of the nominal keyhole; H is the length of the nominal keyhole; L is the left periphery of the nominal keyhole; W is the width of the nominal keyhole; and α is the angle between L and R.)

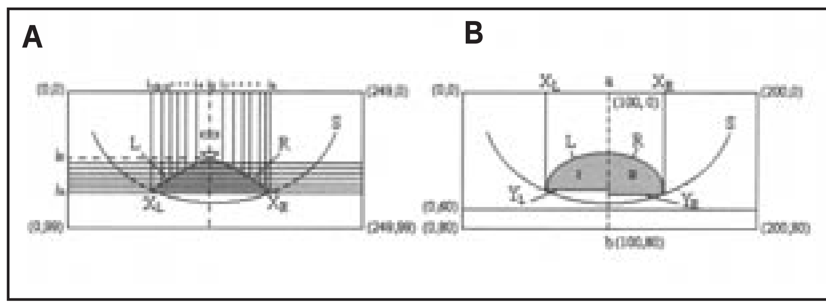

Fig. 6 — Periphery tracing for the nominal keyhole. A — Without wire feed; B — with wire feed.

Image Features of the Keyhole Weld Pool

Keyhole Profile

To better understand a keyhole image, a three-dimensional schematic of a keyhole is shown in Fig. 3. The keyhole is actually a cavity through the weld pool, with a profile resembling a trumpet. The cross section of this cavity varies both in diameter and shape (irregular ellipse). The maximum cross-sectional diameter occurs at the top surface of the workpiece (top section diameter). The cross section with the smallest diameter is located about 1.5–2.5 mm up from the bottom surface of the workpiece (throat section diameter). The diameter of the cross section on the bottom surface of the workpiece is larger than the throat diameter but less than the top section diameter. In uphill welding without wire feeding, the shape of a back-side weld bead is concave-downward along the entire weld path — Fig. 4. Therefore, the keyhole weld pool is a deformed weld pool, and is much different from a weld pool in GTAW and GMAW (Refs. 17–19). However, with wire feeding, the concave-downward shape in the back side of a weld bead will be filled into the convex shape that is a normal full-penetration weld bead.

Image Features

A schematic of a keyhole weld pool without wire feeding and with wire feeding is shown in Fig. 5. The main features of the image are as follows:

1) The images are two-dimensional profiles of the keyhole weld pools projected onto the target plane of the camera, which is defined in this paper as the visual (nominal) keyhole weld pool. This means only a single viewpoint of the keyhole weld pool can be captured by the camera, and the curves in the image are generally in different spatial planes. The pattern of the keyhole weld pool in the image is deformed with respect to the pattern of the actual keyhole weld pool.

2) The front periphery (S) of the nominal keyhole weld pool is clear, but the portion of it at the location with the largest weld bead width cannot be clearly distinguished from the solid area of the base metal. The rear periphery of the nominal keyhole weld pool cannot be seen in the image.

3) The lines L and R are projected lines of the actual periphery of the keyhole. They may be the periphery of the keyhole throat (at the throat cross section [Fig. 3]). However, the periphery S is on the workpiece surface. So, actually, the three curves (L, R and S) are not in the same spatial plane (L and R are not parallel to the workpiece surface). The area bounded by lines L and R and the periphery S is a type of keyhole area through which the plasma arc passes. This area is defined in this paper as the nominal keyhole. With wire feeding, the lines L and R become a smooth curve, and the middle segment of the periphery S is blocked by the cold wire.

4) A highlighted area behind the nominal keyhole exists in the image during a normal welding process. The highlighted area is not the image of the bright arc, but the reflected light from the arc on the rear surface of the weld pool. The area of the nominal keyhole will increase with an increase in the welding current, but the highlighted area will decrease with an increase in welding current. This is because the size of the actual keyhole increases. The area of the nominal keyhole increases to a maximum until the highlighted area vanishes (because there is no surface to reflect the arc light) when the welding process becomes the cutting process.

5) The bright arc cone cannot be seen directly from the image because of the shielding of the torch gas cup.

6) Besides other dimensions of the

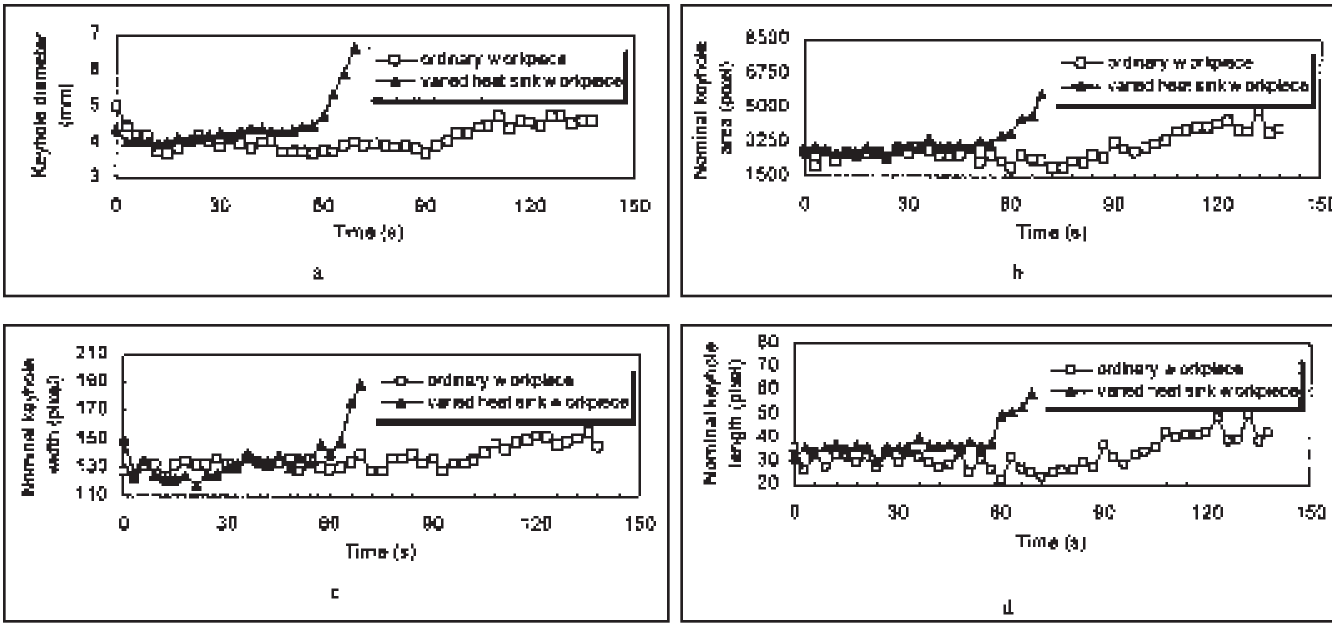

Fig. 7 — Variation of keyhole parameters. A — Bottom diameter of a keyhole; B — nominal keyhole area; C — nominal keyhole width; D — nominal keyhole length.

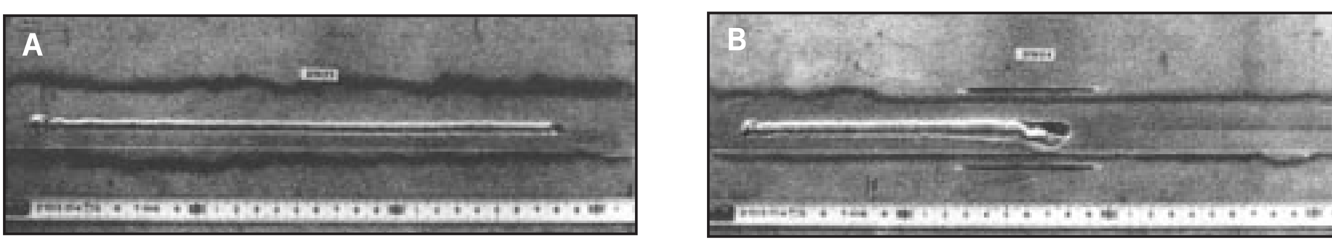

Fig. 8 — Back side photographs of weld beads in butt joints with wire feed. A — Ordinary workpiece; B — varied heat sink workpiece.

nominal keyhole, there are three characteristic points with coordinates (X_L, Y_L), (X_R, Y_R) and (X_O, Y_O) in the image.

7) The quantity of the molten metal in the weld pool with wire feeding is much more than in the case of no wire feeding, so the bottom weld bead profile is convex. This will make the highlighted area in the image become larger than that in the case with wire feeding. However, the image is not as clear as in the case without wire feeding.

Extracting the Nominal Keyhole Periphery

Without Wire Feeding

Because the image of the nominal keyhole weld pool is clear and the difference in grayness between the periphery of the nominal keyhole and the other area is large, no image preprocessing is needed in the case of no wire feed. The characteristic points and the lines of the nominal keyhole can be directly extracted, as shown in Fig. 6A.

The periphery of the nominal keyhole is determined as follows:

- Find the vertical centerline of the highlighted area in the image.
- Determine the starting point for tracing the periphery of the nominal keyhole.
- Trace the periphery of the nominal keyhole.
- Determine the front periphery of the nominal weld pool.

With Wire Feeding

To process the image of a nominal keyhole weld pool, one buffered area of the RAM in the computer is preserved for storing the data of a whole frame of the image sampled per second. The same size area of RAM is preserved for a copy of the data stored in the area of buffer 1. During the data processing of a new sampled image, the data in buffer 1 are changed, but the data in buffer 2 are kept as the initial value. The following simplified algorithm is taken to acquire the area of a nominal keyhole:

1) Within the predefined window, an image frame is divided into two areas separated by the dotted line ab, which is shown in Fig. 6B. The data points to the left of line ab are processed in a sequence from left to right and from top to bottom. In buffer 1, if the gray of a point (x, y) is greater than fifty and the gray difference between this point and the other point (x+5, y+5) is between zero and ten, the gray of the point (x, y) is changed to zero. Otherwise, the original gray of the point (x, y) is saved. The same operation for the data points to the right of line ab is done, but the sequence is from right to left and from top to bottom.

2) The first point with a gray value of zero in each column is searched by scanning the image frame from top to bottom. The left intersecting point between curve S and the nominal keyhole periphery arc L can be located according to the following: to the left of line ab in the image frame, if the ordinates y of the points with

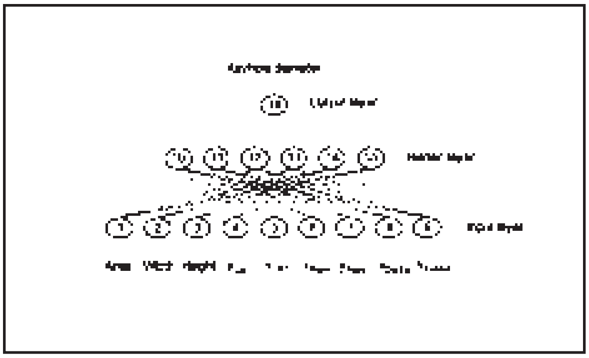

Fig. 9 — Architecture of the BP neural network model of the keyhole diameter.

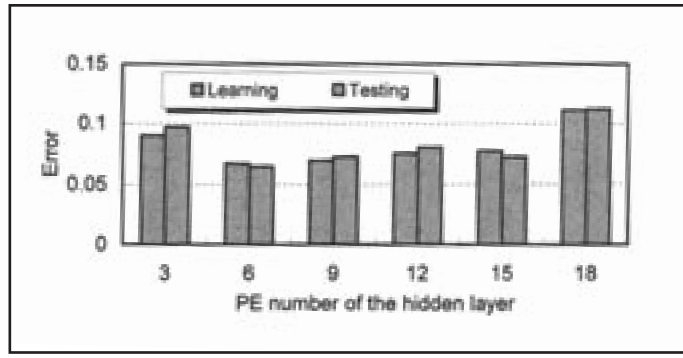

Fig. 10 — Error comparison of the BP neural networks.

the gray value of zero consecutively decrease and the last point among these points has the same abscissa as that of line ab, the first point (x_L, y_L) among these points is the left terminal point of the nominal keyhole periphery L. The right terminal point (x_R, y_R) of the nominal keyhole periphery R can also be acquired by the same method.

3) A straight line Y_L, with ordinate y_L to the left of line ab and perpendicular to the Y axis, is drawn. Another straight line, Y_R, can be drawn in a similar way. The area I, surrounded by lines ab, L and Y_L, and the area II, surrounded by lines ab, R and Y_R, are added together to represent the nominal keyhole area.

The other geometrical size (width and length) of a nominal keyhole and the coordinates of the points (X_L, Y_L), (X_R, Y_R) and (X_O, X_O) can also be calculated according to their number of pixels and their corresponding gray values in the image frame.

Variation of a Keyhole

Many factors — arc stability, energy input of a workpiece, flow rates of gases, position and speed stability of the wire feed, thermal condition variations generated by the workpiece structure and heat buildup because of the continuous welding process itself — may influence the transition from a normal keyhole welding process to a cutting process or a melt-in mode welding process. The variation in thermal conditions is the most crucial and complex among these factors because of its variability, immeasurability and uncontrollability. In keyhole welding, the cutting process usually occurs more easily than in the melting-in mode welding process. Once a cutting process occurs, the weld bead is not acceptable and must be repaired. Thus, avoiding a cutting process resulting mainly from a variation in thermal conditions is a high priority. This is also one of the prerequisites for achieving a uniform and stable weld formation.

In essence, the reason for generating a cutting process is that not enough metal exists in the weld pool and too much energy is deposited in the workpiece. The experiments reported in this paper show that under constant energy input, when the thermal condition of a workpiece is changed due to the buildup of heat, the keyhole size becomes larger as the weld pool becomes wider. When the keyhole size is larger than a certain value, a cutting process will be generated. To avoid this melt-through mode cutting process, the quantity of the filler metal should be increased, which will decrease the size of the keyhole even though the width of the weld bead generated will probably be larger than that of a normal keyhole weld bead. Figure 7 shows the relationship of the bottom diameter of a keyhole and the nominal keyhole size to the time using the workpieces shown in Fig. 2, in which the origin of the time axis represents the instant when the work-

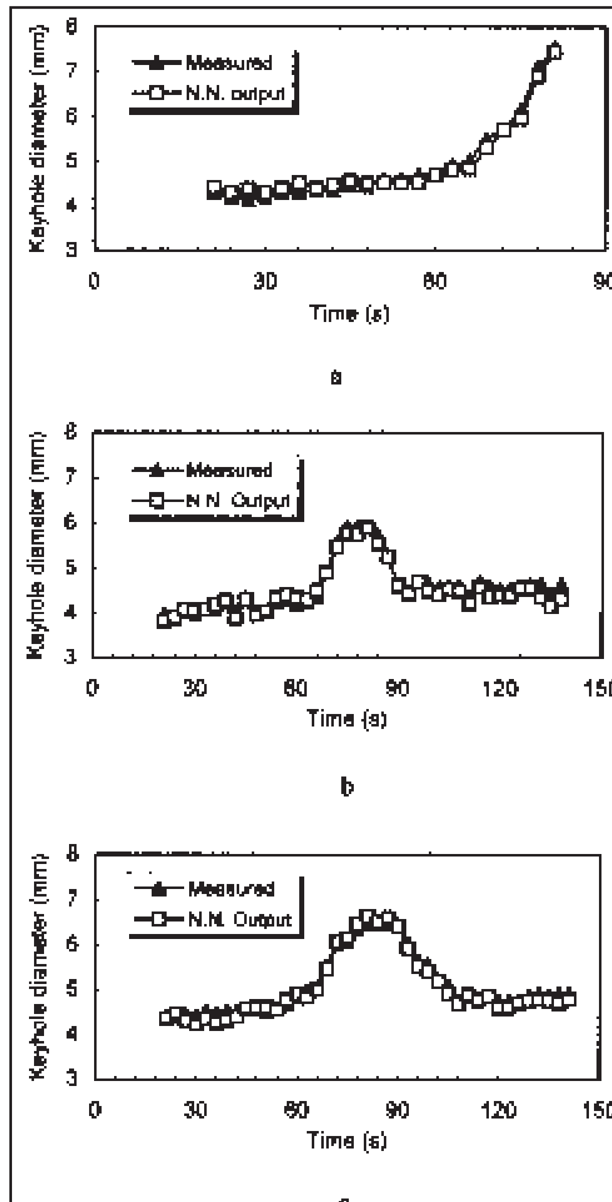

Fig. 11 — Bottom diameters of a keyhole from neural net output and actual measurement. A — Constant welding parameters; B — variable welding current; C — variable wire feed speed.

Table 1 — Welding Parameters for BP Neural Network Modeling of the Bottom Diameter of a Keyhole with Wire Feeding

Number of experiment	Slot length (mm)	Welding current (A)	Wire feed speed (mm/s)
1	0	97	14
2	0	97	15
3	6	97	15
4	6	97–87–97	15
5	6	97–92–97	15
6	6	97	15–17–15
7	6	97	15–19–15
8	6	97	15–21–15
9	6	97–92–97	15–19–15
10	6	97–92–97	15–21–15
11	6	97–87–97	15–17–15
12	6	97–87–97	15–19–15

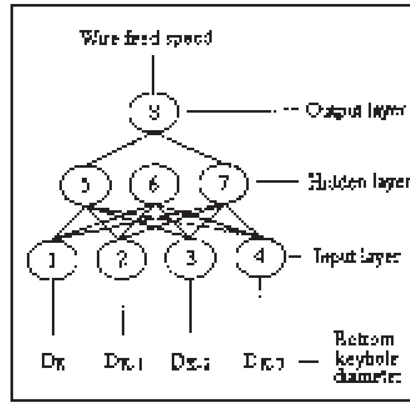

Fig. 12 — Control model of the bottom diameter of a keyhole.

piece movement is initiated after the keyhole size reaches a certain value. Because it is not currently possible to synchronously measure the bottom diameter of a keyhole in a welding process, the off-line measured width between the bottom oxide films along a weld bead, which is the trace of the arc efflux, is used for representing the bottom diameter of a keyhole. To accurately acquire the data, marks with an interval of 1.0 mm are made on the top and bottom faces along the butt-jointed workpieces before welding. The cycle of image sampling is 1.0 s and the welding speed is 6.48 m/h. Therefore, the measuring interval is 1.8 mm. Associated with the corresponding photos given in Fig. 8, the following results were obtained:

1) The bottom diameter of the keyhole on the ordinary workpiece increases with time during the first 20 s — Fig. 7A. However, at the nearby origin, it is about 4.5–5.0 mm because of the arc preheat at the start location, and then decreases to 3.8 mm because of the better heat transfer conditions of the workpiece after torch motion is initiated. From that instant, the bottom is nearly constant in the range of 3.8 to 4.0 mm up until 90 s. From about 90 s, it increases to 4.5 mm because of the heat buildup and maintains 4.5 mm after 110 s. Therefore, the keyhole welding process can enter a stable state after 20 s from the start, during which the variation of the keyhole diameter is 0.2 mm up to 100 s. For the varied heat sink workpiece, it can also be seen the keyhole diameter has nearly the same variation as that of the ordinary workpiece up until 30 s, even though there exists a small difference during the first 10 s. Because the thermal condition is getting worse after 30 s (the arc is reaching the area with a slot machined on each workpiece), the variation of the keyhole diameter rapidly increases to more than 6.8 mm at the instant of 72 s. After that, the keyhole welding process becomes the cutting process.

2) The geometrical size (the area, width and height are shown, respectively, in Fig. 7B–D) of the nominal keyhole in an image has the same trend as the bottom diameter of the keyhole, for both the ordinary and the varied heat sink workpiece, even though there are some slight differences between them. The change in the area shows the largest variation among these characteristic sizes. However, all this size data cannot represent the variation in the bottom diameter of a keyhole, which is actually a measurement of the full-penetration state. Thus, to avoid the cutting process, the bottom diameter of a keyhole should be correlated with the geometrical size of the nominal keyhole.

3) The allowable magnitude of the variation in the bottom diameter of a keyhole is not large (± 2.0 mm). The time interval required for the welding process to become the cutting process for nominal welding velocities of 100 mm/min shows the response time for both acquiring and processing the image and for controlling the full weld penetration should be less than 20 s.

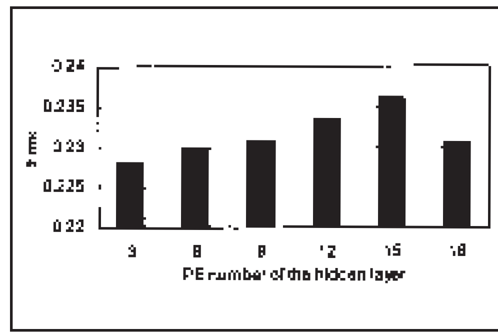

Fig. 13 — Training error of the BP neural network.

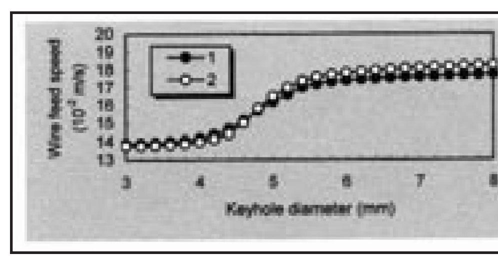

Fig. 14 — Output of the controlling model of the wire feed speed. (Note: curve 1 is the output of the model using the data from open-loop control experiments; curve 2 is the output of the model using the data from closed-loop control experiments.)

Modeling the Keyhole Diameter

The following experiments were made for mapping the relationship of the bottom diameter of a keyhole with the geometrical size of the corresponding nominal keyhole in an image:

1) Ordinary workpiece with constant welding parameters.

2) Varied heat sink workpiece with constant welding parameters.

3) Varied heat sink workpiece with a variation in wire feed speed.

4) Varied heat sink workpiece with a variation in welding current.

5) Varied heat sink workpiece with variations in both the welding current and the wire feed speed.

The purpose of the variations in the welding current and/or the wire feed speed is to maintain a continuous welding process and prevent an occurrence of a cutting process. The parameters applied are shown in Table 1. As an example of experiment 4, the welding current is maintained at an initial value of 97 A until the area with the varied heat sink is reached. Then the welding current is stepped down to 87 A. When the area with the varied heat sink is passed, the welding current is stepped up again to 97 A. In experiment 6, the initial wire feed speed is maintained at a value of 15 cm/s until the area with the varied heat sink is reached. Then it is increased to a maximum value of 17 cm/s according to a slope at the middle location of the area with the varied heat sink. After that, it is decreased to the initial value of 15 cm/s according to a slope. Every experiment is repeated four times. The first three of the same four experiments are used for model recognition, and the last experiment is for verifying the accuracy of the model established based on the three experiments. Every group of parameters associated with the results of the image processing is recorded once a second, 20 seconds after the weld initiation. From the three groups of experiments in Table 1 (from 1 to 4, 5 to 8 and 9 to 12), 3855 groups of data were acquired.

An artificial BP neural network of three layers with nine parameters as inputs and the bottom diameter of a keyhole as an output, which can implement any map from m dimensions to n dimensions, was used to model the system — Fig. 9. As the number of hidden layers is not easily determined using current theories, the BP models with one hidden layer consisting of elements of 3, 6, 9, 12, 15 and 18 are respectively examined using the Gauss initiation procedure and the Delta rule (Ref. 24). Figure 10 shows the error comparison of the models with different layers. A comparison of the neural network output with the measured results is given in Fig. 11. It can be seen the training error of the model is the smallest value of 6.77%, and the corresponding error of the experiment examined is 6.64% when the number of the hidden layer element is selected as six. Also, the corresponding curves measured and output from the model agree well with each other. Thus, the model with a six-element hidden layer was selected as the mapping model between the bottom diameter of a keyhole and the geometrical size of a corresponding nominal keyhole, as well as the three pairs of coordinates in the image schematically shown in Fig. 5. However, the model should be retrained using new experimental data if the thickness of a workpiece and different welding parameters are applied.

Real-time Feedback Control of the Full Weld Penetration

As stated above, the reason for the occurrence of a cutting phenomenon is not enough metal is inside the weld pool. To guarantee full penetration control and achieve a uniform weld bead, the quantity of the weld pool metal should be controlled. Based on the fact the keyhole size may be regulated by adjusting the wire feed speed and the heat input may be controlled by changing the welding current, the wire feeding speed was selected as the first controlling variable for full weld penetration.

Controlling Model

To model the relationship between the wire feed speed and the bottom diameter of a keyhole by the black-box method, the artificial BP neural network theory was applied. Because the welding process is a time delay process (the response of the weld pool status to the adjustment of the controlling parameters takes a longer

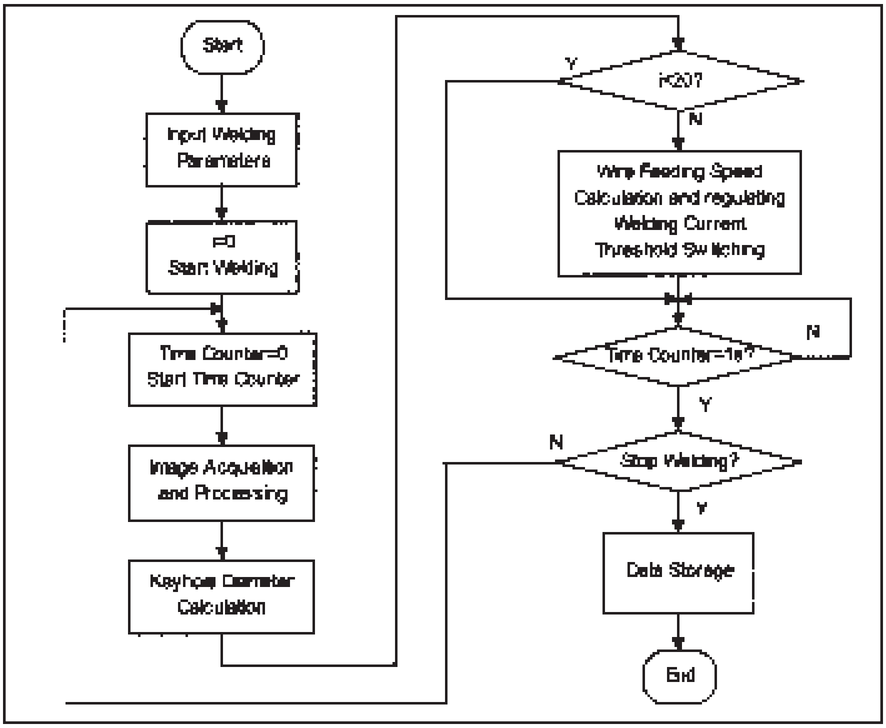

Fig. 15 — Block diagram of the program for closed loop control of full penetration in butt-jointed plates.

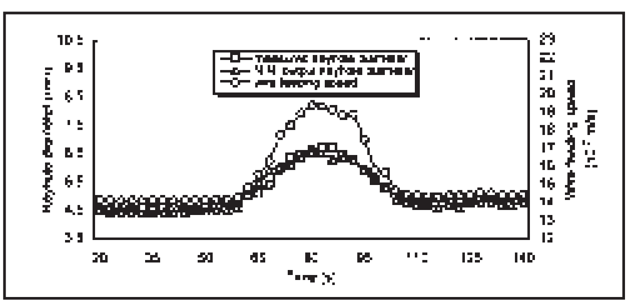

Fig. 16 — Bottom diameter of a keyhole and wire feed speed vs. the time in the full penetration control of a weld bead in a butt joint using wire feed speed as a control variable.

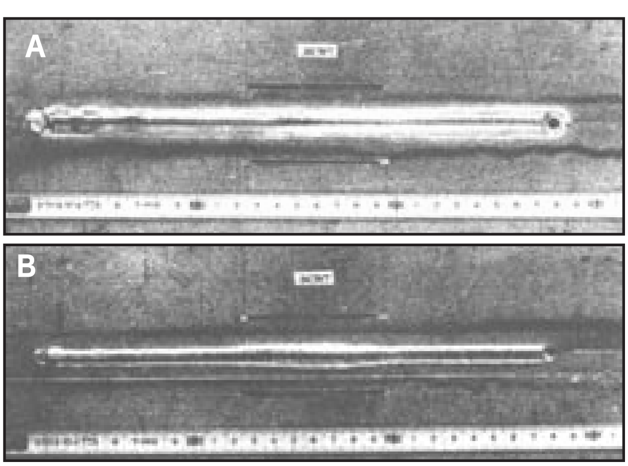

Fig. 17 — A weld bead with closed loop control of full penetration in a butt joint using wire feed speed as a controlling variable. A — Top face; B — bottom face.

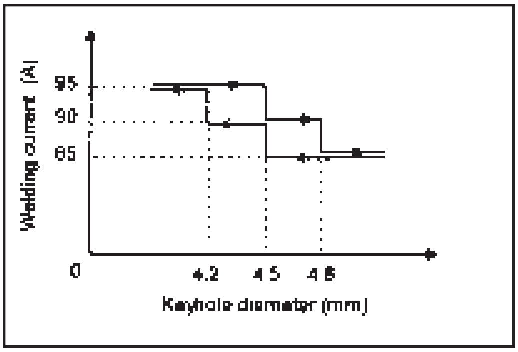

Fig. 18 — Schematic of the welding current regulation.

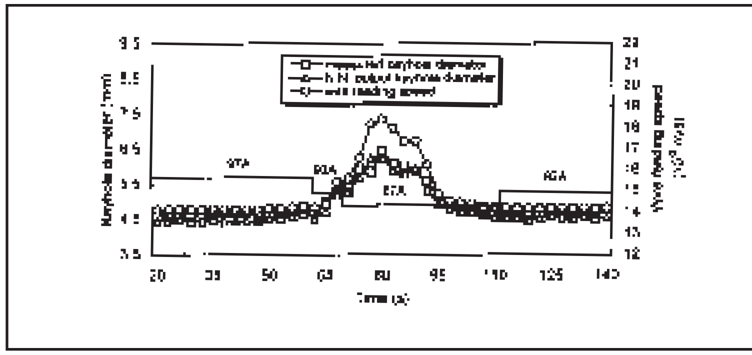

Fig. 19 — Bottom diameter of a keyhole, welding current and wire feed speed vs. the time in the full penetration control of a weld bead in a butt joint using wire feed speed and welding current as controlling variables.

time), the previous data values for the input should be utilized in the establishment of a model using current data value. A model of three layered BP neural networks was established, with the current wire feed speed as the output and the current and previous bottom diameters of the keyholes as the input. The number of hidden layer elements is selected from the experiments. In the beginning, the training sample data are acquired from the experiments in Table 1 when the wire feed speed was changed. So, two categories of data (associated with the varied heat sink workpiece and the ordinary workpiece, respectively) are selected according to the standard: there is no apparent concave or undercut in a weld bead. The bottom diameter of a keyhole, which is the input for the controlling model shown in Fig. 12, is the output in Fig. 9. From the comparison of the output results of the neural networks model with the training sample data, illustrated in Fig. 13, it can be seen the model with three elements in the hidden layer has the smallest error. Also, the difference between the output results of the neural networks model and the training sample data is large. The reason for this is the changes in the wire feed speed are limited and the standard for an acceptable weld bead is not very strict. Consequently, contradictory data are included in the training data sample collection.

In Fig. 14, curve 1 is the model output of the wire feed speed regulator based on the above data sample collection used for training the model. The corresponding initial and terminal data values, as well as the increment value of the bottom diameter of a keyhole are respectively 3.0, 8.0 and 0.1 mm. Curve 2 is the output of the same regulator trained using the new data sample collection acquired from the feedback experiments done under the condition of the varied heat sink according to curve 1. These experiments are divided into three groups: the first four experiments are for constant welding current; the second four experiments are for a decrease in welding current by 5 A when the area with a slot is reached; the last four experiments are for a decrease in welding current by 10 A when the heat sink of the workpieces is increased.

According to the feedback control theory, it can be seen the regulator in Fig. 12 can regulate the wire feed speed to change the keyhole size depending on the variation in the keyhole diameter, so an occurrence of the cutting process may be avoided.

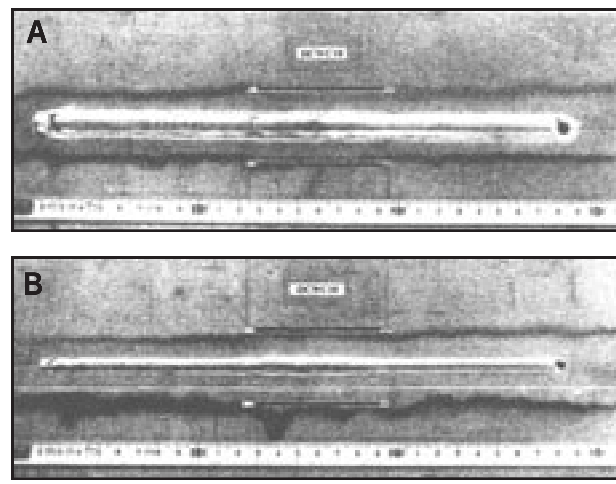

Fig. 20 — A weld bead in a butt joint with the closed-loop control of weld formation using both wire feed and welding current as controlling variables. A — Top face; B — bottom face.

Full Penetration Control

The block diagram of the program for controlling full penetration of a weld bead for the butt-joint plates is shown in Fig. 15. Because a welding process needs about 20 s to enter the stable main body segment from the start-up segment, the control process of the full penetration begins at the 20th cycle of the image sampling (*i.e.*, the control strategy is applied after the variable I equals 19 s in Fig. 15).

The wire feed speed and the bottom diameter of a keyhole are recorded, measured and calculated, the relationships of which, versus time, are shown in Fig. 16. The corresponding photograph of a weld bead is given in Fig. 17. It shows the following:

• The cutting process can be avoided reliably using the wire feed speed as a controlling variable in the real-time closed loop control of the full weld penetration when the thermal condition of the workpiece changes.

• In the areas with a poorer heat sink because of the slots, the width and height of the bottom weld bead are apparently wider and higher than those in other areas with a better heat sink. The corresponding width of the top bead is a little wider and the corresponding height of the top bead is a little reduced. However, there are no concave or undercut defects in the weld bead.

• The weld formation is not uniform.

Optimization of the Weld Formation

To achieve a uniform weld formation during the full weld penetration control process, the welding current should be controlled for regulating the heat input to the workpiece. Although the experiments show the cutting process can also be avoided by adjusting only the welding current, there often exist undercut and concave defects in the top weld bead.

A solution that includes the regulation of the wire feed speed is shown in Fig. 18. Three thresholds of the bottom keyhole diameters of 4.3, 4.6 and 5.1 mm are respectively matched with the welding current of 97, 92 and 87 A. The changing mode of the welding current is designed into the following:

1) When the bottom diameter of a keyhole increases to a threshold, the welding current is decreased according to the top downstairs-shaped curve in Fig. 18.

2) When the bottom diameter of a keyhole decreases to a threshold, the welding current is increased according to the bottom upstairs-shaped curve.

3) When the bottom diameter of a keyhole changes between the two neighboring thresholds and does not reach those thresholds, the welding current is held constant. To weaken the influence of any noise during an on-line control process, an average-weighted filtering method is applied to the determination of the bottom diameter of a keyhole: the weighted coefficients are 0.5, 0.3 and 0.2, respectively, for the current diameter, the former diameter and the diameter before the former diameter.

Figure 19 shows the responses of the welding current and the wire feed speed to the variation in the bottom diameter of a keyhole during a real-time feedback control process. Compared with the results in Fig. 16, it can be seen the bottom diameter becomes significantly smaller in area with a poorer heat sink because of the slots and the quantity of wire feed is decreased to avoid a cutting process. The corresponding photograph of the weld bead (Fig. 20) also shows the bead is more uniform than that in Fig. 17. Therefore, a combination of the wire feed regulation with welding current adjustment can further improve the weld formation in VPPAW of aluminum alloys by the keyhole mode.

Conclusions

The following conclusions can be made based on the results of this study:

1) A clear image of the keyhole weld pool can be obtained using a band-pass filtering method. The nominal keyhole in the image is a part of the actual keyhole, the geometrical features of which can reflect the variation in the bottom diameter of a keyhole regardless of whether there is wire feed or not.

2) The main reason for an occurrence of a cutting phenomenon is not enough metal is appropriately added to the weld pool during a welding process. The development of a cutting process from a keyhole welding process takes some time, which allows full weld penetration control.

3) The model, established between the bottom diameter of a keyhole and the geometrical size of a nominal keyhole weld pool in the image, effectively and accurately reflects the keyhole variation. The bottom diameter of a keyhole can be used as a characteristic parameter to monitor and control the full weld penetration.

4) The model for controlling the full weld penetration can be applied to a welding process using the wire feed speed as a control variable to reliably avoid an occurrence of a cutting process or a melt-in mode. However, a uniform weld bead may not be obtained by using only the wire feed speed as a single controlling variable.

5) Uniform weld formation can be achieved using a combination of the wire feed speed regulation with welding current adjustment according to the variation in the bottom diameter of a keyhole in the full weld penetration control of a weld bead.

6) The approach used in this paper should be further explored when thicker materials are applied. The influence of the arc light intensity should be a greater condition when designing a filtering system under the condition of a high welding current.

Acknowledgments

The authors wish to acknowledge the financial support from the National Key Laboratory of Advanced Welding Production Technology at Harbin Institute of Technology, P. R. China, and from the National Science Foundation (Project Nos. DMI-9900011 and DMI-9700102).

References

1. Nunes, A. C. 1984. Variable polarity plasma arc welding on space shuttle external tank. *Welding Journal* 63(4): 27-s to 35-s.

2. Woodward, H. A. 1996. U.S. contractor for the international space station. *Welding Journal* 75(3): 35-s to 40-s.

3. Torres, M. R. 1992. Gas contamination effects in variable polarity plasma arc welded aluminum. *Welding Journal* 71(4): 123-s to 130-s.

4. Martinez, L. F. 1994. Effect of weld gases on melt zone size in VPPA welding of Al 2219. *Welding Journal* 73(10): 50-s to 55-s.

5. Martinez, L. F. 1992. Front side keyhole detection in aluminum alloys. *Welding Journal* 71(5): 49-s to 52-s.

6. Steffens, H. D. 1972. Automatic control for plasma arc welding with constant keyhole. *Welding Journal* 51(6): 40-s to 45-s.

7. Metcalfe, J. C., and Quigley, M. B. C. 1975. Keyhole stability in plasma arc welding. *Welding Journal* 54(11): 401-s to 404-s.

8. Zhang, J. H., and Wang, Q. L. 1985. Study on arc sound in TIG and plasma processes. *IIW Doc. 212-610-85.*

9. Hu, B. X. 1980. The study of controlling system of welding quality at all-positions by using the arc sound in pulsed plasma arc welding of steel. *Welding* 3: 17–20

10. Agapakis, J. E., and Bolstad, J. 1991. Vision sensing and processing system for monitoring and control of welding and other high luminosity processes. *Proc. of the International Robots & Vision Automation Conference*, pp. 23–29.

11. Nakata, S, Huang, J., and Tsuruha, Y. 1988. Visual sensing system for in-process control of arc welding process. *Welding International* 12: 1086–1090.

12. Hoffman, T. 1991. Real-time imaging for process control. *Advanced Materials & Processes* 9: 37 to 43.

13. Guu, A. C., and Rokhlin, S. I. 1989. Computerized radiographic weld penetration control with feedback on weld pool depression. *Materials Evaluation* 10: 1204–1210.

14. Guu, A. C., and Rokhlin, S. I. 1992. Arc weld process control using radiographic sensing. *Materials Evaluation* 11: 1344– 1348.

15. Rokhlin, S. I., and Guu, A. C. 1990. Computerized radiographic sensing and control of an arc welding process. *Welding Journal* 69(3): 83-s to 95-s.

16. Richardson, R. W., and Gutow, D. A. 1984. Coaxial arc weld pool viewing for process monitoring and control. *Welding Journal* 63(3): 43-s to 50-s.

17. Kovacevic, R., and Zhang, Y. M. 1993. Three-dimensional measurement of weld pool surface. *Proc. of the International Conference on Modeling and Control of Welding Processes,* Fla.

18. Kovacevic, R., and Zhang, Y. M. 1995. Vision sensing of 3D weld pool surface. *Proc. of the 4th International Conference on Trends in Welding Research*, Gatlinburg, Tenn.

19. Kovacevic, R., and Zhang, Y. M. 1996. Monitoring of weld penetration based on weld pool geometrical appearance. *Welding Journal* 75(10): 317-s to 329-s.

20. Nagarajan, S., Chen, W. H., and Chin B. A. 1989. Infrared sensing for adaptive arc welding. *Welding Journal* 68(11): 462-s to 466-s.

21. Nagarajan, S., Banerjee, P., Chen, W. H., and Chin, B. A. 1990. Weld pool size and position control using IR sensors. *Proceedings of NSF Design and Manufacturing Systems Conference*. Arizona State University.

22. Chen, W., and Chin, B. A. 1990. Monitoring joint penetration using infrared sensing techniques. *Welding Journal* 69(4): 181-s to 185-s

22. Oshima, K., and Morita, M. 1992. Sensing and digital control of weld pool in pulsed MIG welding. *Transactions of the Japan Welding Society* 23(4): 36–42.

23. Hagan, M. T., Demuth, H. B., and Beale, M. 1996. *Neural Network Design*. PWS Publishing Co., pp. 1–43.